Design and Implementation of the Off-Line Robust Model Predictive Control for Solid Oxide Fuel Cells

Authors:

Narissara Chatrattanawet, Soorathep Kheawhom, Yong-Song Chen, Amornchai Arpornwichanop

Date Submitted: 2020-01-07

Keywords: control synthesis, off-line calculation, robust model predictive control, solid oxide fuel cell

Abstract:

An off-line robust linear model predictive control (MPC) using an ellipsoidal invariant set is synthesized based on an uncertain polytopic approach and then implemented to control the temperature and fuel in a direct internal reforming solid oxide fuel cell (SOFC). The state feedback control is derived by minimizing an upper bound on the worst-case performance cost. The simulation results indicate that the synthesized robust MPC algorithm can control and guarantee the stability of the SOFC; although there are uncertainties in some model parameters, it can keep both the temperature and fuel at their setpoints.

Record Type: Published Article

Submitted To: LAPSE (Living Archive for Process Systems Engineering)

Citation (overall record, always the latest version):	LAPSE:2020.0058
Citation (this specific file, latest version):	LAPSE:2020.0058-1
Citation (this specific file, this version):	LAPSE:2020.0058-1v1

DOI of Published Version: https://doi.org/10.3390/pr7120918

processes

MDPI

Article

Design and Implementation of the Off-Line Robust Model Predictive Control for Solid Oxide Fuel Cells †

Narissara Chatrattanawet [1], Soorathep Kheawhom [1], Yong-Song Chen [2] and Amornchai Arpornwichanop [1,*]

[1] Center of Excellence in Process and Energy Systems Engineering, Department of Chemical Engineering, Faculty of Engineering, Chulalongkorn University, Bangkok 10330, Thailand; narissara_hl@hotmail.com (N.C.); soorathep.k@chula.ac.th (S.K.)

[2] Advanced Institute of Manufacturing with High-Tech Innovations and Department of Mechanical Engineering, National Chung Cheng University, Chiayi 62102, Taiwan; imeysc@ccu.edu.tw

* Correspondence: amornchai.a@chula.ac.th

† This paper is an extended version of paper presented at the 12th Process Systems Engineering (PSE) and 25th European Symposium of Computer Aided Process Engineering (ESCAPE), Copenhagen, Denmark, 31 May–4 June 2015.

Received: 14 September 2019; Accepted: 23 November 2019; Published: 3 December 2019

Abstract: An off-line robust linear model predictive control (MPC) using an ellipsoidal invariant set is synthesized based on an uncertain polytopic approach and then implemented to control the temperature and fuel in a direct internal reforming solid oxide fuel cell (SOFC). The state feedback control is derived by minimizing an upper bound on the worst-case performance cost. The simulation results indicate that the synthesized robust MPC algorithm can control and guarantee the stability of the SOFC; although there are uncertainties in some model parameters, it can keep both the temperature and fuel at their setpoints.

Keywords: solid oxide fuel cell; robust model predictive control; off-line calculation; control synthesis

1. Introduction

A solid oxide fuel cell (SOFC) is a promising fuel cell technology that can be used in co-generation systems for widespread commercial applications [1]. No moving parts, quiet operation, low pollution, and high efficiency are the advantages of fuel cells. Many researchers have discussed the considerable environmental benefits of fuel cell technology [2]. Using SOFC technology also involves the depletion of greenhouse gas emissions when compared with traditional energy generation methods. Moreover, there is interest in the development of the fuel cell technology as a substitute for internal combustion [3]. In general, a SOFC is operated over a wide temperature range, from 873–1273 K, which leads to high energy conversion efficiency, fuel flexibility, and the possibility for combined heat and power systems [4].

The SOFC can use various fuel types, such as methane, methanol, ethanol, and other hydrocarbons, due to its high operating temperature range. Even though high-chain hydrocarbons, such as n-dodecane, can be used as a fuel for the SOFC system, methane is generally considered for SOFC operation, due to its availability, highest hydrogen to carbon ratio in hydrocarbon substances and low cost [5,6]. As the long-chain hydrocarbon fuel contains high carbon and it has a low hydrogen-to-carbon ratio, fuel processing is required for breaking this fuel down into small substances and increasing the hydrogen-to-carbon ratio for the avoidance of a carbon formation in SOFC [7]. In general, methane can be synthesized, as a major product or a by-product, from many chemical processes, or even formation process [8]. In addition, methane in biogas can be directly fed to SOFC under dry conditions; however,

there is a risk that is associated with contaminants in biogas when it is introduced to commercial SOFCs while using Ni-YSZ anode [9,10]. Therefore, either commercialized material development or fuel processing with cleaning technologies is required. There are many hydrogen production processes to convert methane into hydrogen-rich gas, such as steam reforming, partial oxidation, and autothermal reforming. However, the methane steam reforming process is perhaps the most well-established technology and it is widely used to produce hydrogen in the conventional SOFC system [11]. Internal reforming process can occur within the fuel cell to directly convert hydrocarbon fuel into hydrogen-rich gas since SOFC is operated at high temperatures [12]. The direct internal reforming (DIR) includes the reforming and water gas shift reaction rates and enthalpies, with these reactions occurring on the surface of the anode. The DIR of methane in an anode of the SOFC can possibly be due to the high temperatures that are present in the SOFC anode and it enables high energy conversion efficiency for the system [13]. However, the complete DIR-SOFC showed poorer performance when compared to the DIR-SOFC with partial external reforming, and thus using the pre-reformer with DIR-SOFC might be a suitable operational option [14]. Nevertheless, the internal reforming reaction that occurred at the anode leads to complicated dynamic behavior. Additionally, the steam reforming process is a highly endothermic reaction [15]. The endothermic cooling effect creates a temperature gradient inside the fuel cell stack. The thermal gradient in the cell stack is significantly managed to minimize, because this gradient results in thermal stresses that leads to cell degradation and failure [16,17]. Consequently, efficient control is needed for preventing thermal cracking and ensuring system stability for this process.

The model of SOFC in cell, stack, and system levels has been proposed, and each type of the SOFC model is employed for different purposes, i.e., design, improvement, control, and optimization [18]. Dynamic modeling is especially beneficial for dynamic system analysis, as well as in control design. SOFC operations are often subjected to transient conditions, and, as a result, the fuel cell dynamics have been increasingly considered in modeling activities [19]. Several published works have concentrated on the dynamic modeling and the control of solid oxide fuel cells [20,21]. Li and Choi [22] studied the control of the power output of an SOFC by applying proportional-integral (PI) controllers to maintaining fuel utilization and voltage as the current of the stack changed. To keep the voltage output under load changes, Chaisantikulwat et al. [19] developed an SOFC dynamic model and a feedback control scheme with a PI controller to control cell voltage by manipulating the concentration of H_2. The low-order dynamic model that was derived from the step responses was used for designing feedback control. The results showed that the feedback PI controller was able to maintain a constant SOFC voltage for small step changes in the current load. Furthermore, a dynamic model was used to investigate the dynamics of the SOFC stack and design control strategies [23]. A proportional-integral-derivative (PID) controller was implemented to maintain the outlet fuel temperature and the fuel utilization of a planar anode-supported, direct internal reforming solid oxide fuel cell under intermediate-temperature operation. The feed air was used to maintain the outlet fuel temperature when a disturbance in the current density occurred. A control strategy must be more effective in avoiding oscillatory control action as well as in preventing potentially damaging temperature gradients under a higher magnitude of load changes. Stiller et al. [24] developed a dynamic model for the control of an SOFC and gas turbine hybrid system. The SOFC power, fuel utilization, air flow, and cell temperature were controlled while using a proportional–integral–derivative (PID) type controller. However, the conventional PID controller cannot guarantee stability and performance when large disturbances occur.

Model predictive control (MPC), which is a multivariable control algorithm, computes a controller action while using a process model to predict the processes output trajectory in the future [25]. The implementation of MPC requires the identification of an internal process model. Therefore, applying model-based controllers, such as MPC, is more challenging when compared to PI or PID controllers for which explicit controller equations exist [26]. Zhang et al. [25] developed the nonlinear MPC controller (NMPC) for a planar SOFC while using the moving horizon estimation (MHE) method. The current density and molar flow rates of fuel and air were manipulated variables to

control the output power, fuel utilization, and cell temperature. The proposed NMPC controller can drive the SOFC following the desired output trajectory when the power output was changed under constant fuel utilization and temperature. In addition, many real chemical processes involve a high degree of parameter uncertainty. Some studies have focused on the development of a robust MPC to handle nonlinear systems and guarantee system stability, as a traditional MPC algorithm is unable to address plant model uncertainties [27,28]. Kothare et al. [29] synthesized a robust MPC algorithm that explicitly incorporated plant model uncertainties. The state feedback control law was obtained by minimizing the worst-case performance cost. This worst-case scenario was used by the simultaneous design and control methodologies to evaluate the process cost function and constraints that were considered in the process [30]. Manthanwar et al. [31] studied the derivation of the explicit control strategy while using a min–max formulation to safeguard against the worst-case uncertainty problem. This guarantee process feasibility as well as process stability for efficient plant operation. A convex optimization problem with linear matrix inequalities (LMIs) constraints was formulated. Bumroongsri and Kheawhom [32] proposed a robust MPC for uncertain polytopic discrete-time systems. In addition, an ellipsoidal off-line MPC strategy for linear parameter varying (LPV) systems was studied. The smallest ellipsoid that contained the present measured state was determined in each sequence of ellipsoids and the scheduling parameter for LPV was measured on-line. Pannocchia [33] also developed a robust MPC algorithm to stabilize the system that was described while using a linear time-varying (LTV) model. Kouramas et al. [34] focused on the design of an MPC controller to control the cell voltage and cell temperature. The results showed that the controller was able to maintain the SOFC voltage and temperature at the desired values. A comprehensive model of SOFC behavior involves numerous complex phenomena, which include electrochemical reaction and the thermal and mechanical properties of the materials. Thus, the SOFC model involves a great deal of parameter uncertainty; the control design should take the model uncertainty into account. For an on-line synthesis approach, the optimization requirement leads to significant amounts of on-line MPC computational time. When MPC incorporates the model uncertainty, the resulting on-line computation will significantly grow with the number of vertices of the uncertainty set. As a result, an off-line synthesis approach is a focus for generating a robust MPC for an uncertain model. With the off-line approach, the computation of a robust MPC is significantly reduced, with only minor losses in its control performance. Wan and Kothare [35] implemented an off-line LMIs for robust MPC while using an asymptotically stable invariant ellipsoid. An off-line robust output feedback MPC approach can certify the robust stability of the closed-loop system in the presence of constraints and it can stabilize both polytopic uncertain systems and norm bound uncertain systems.

A model-based control system should be designed, while taking uncertain parameters into account, to avoid physical damage and achieve high energy efficiency, as the dynamics of SOFC, especially with a DIR operation, are complicated and its model consists of many key parameters. This study concentrates on control design for the DIR SOFC fed by methane-rich gas. The investigation of transient responses of an SOFC by changing the current density, the air and fuel inlet temperatures, and the air and fuel inlet molar flow rates in terms of velocity, is reported. A MIMO control approach using an off-line robust MPC algorithm with LTV system is implemented to control the SOFC with uncertainty in cell voltage. The paper is organized, as follows: Section 2 presents the mathematical model for the SOFC; Section 3 gives a brief review of the robust MPC algorithm; Sections 4 and 5 outline the application, and results and discussion of the proposed off-line robust MPC to the SOFC; and lastly, Section 6 presents the conclusions.

2. SOFC Model

The mathematical model of the solid oxide fuel cell (SOFC) consists of mass balances, energy balances, and the electrochemical model. The assumptions for the lumped model of the SOFC are as follows: (i) heat loss to the surroundings is negligible; (ii) all the gases are ideal gas; (iii) pressure

gradients inside gas channels are negligible; (iv) the heat capacity of all gases is temperature independent; and, (v) the exit fuel and air temperatures and the cell temperature are the same.

Typically, the SOFC consists of a ceramic ion-conducting electrolyte and two porous electrodes with a sandwich structure (Figure 1). To generate electricity with an SOFC, methane-rich gas is directly fed into the anode side while air, which is the oxidant, is continuously delivered into the cathode side. At the cathode side, oxygen is reduced, which forms oxygen ions. The oxygen ions can diffuse through the ion-conducting electrolyte to the anode/electrolyte interface. At the anode side, the oxygen ions chemically react with hydrogen in the fuel, producing water and electrons. The electrons are transported via the external circuit and back to the cathode/electrolyte interface, thus producing electrical energy. Exhaust gases and heat are also produced by the SOFC as by-products. The reforming, electrochemical, and energetic models are simultaneously solved to obtain an exact solution [36].

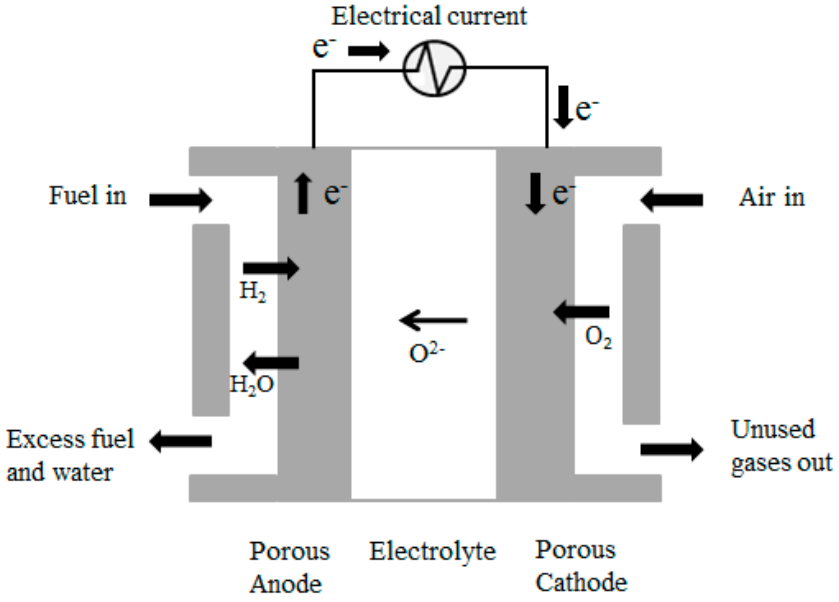

Figure 1. Schematic diagram of solid oxide fuel cell operation.

2.1. Mass and Energy Balances

The internal methane steam reforming (MSR) reaction in porous-supported SOFC is the most important factor for determining the performance of the SOFC [37]. Furthermore, it is the main reaction for hydrogen production. Table 1 shows the reactions that occurred within the SOFC, which include steam reforming, water-gas shift (WGS), and overall redox reaction [38]. These reactions are used in mass and energy balances. In the fuel channel, it is assumed that methane can only be reformed to hydrogen, carbon monoxide, and carbon dioxide and, therefore, cannot be electrochemically oxidized [23]. In the endothermic steam reforming reaction, fuel in the presence of a catalyst produces hydrogen and carbon monoxide. Table 1 shows the rate expression of the steam reforming reaction $R_{(i)}$ [38], where k_0 is the pre-exponential constant, being equal to 4272 mol s^{-1} m^{-2} bar^{-1}, and E_a is the activation energy, equal to 82 kJ mol^{-1}. Excess steam is used to prevent carbon formation on the catalyst and force the reaction to completion. An associated reaction to the reforming reaction is the water-gas shift reaction. Unlike the steam reforming reaction, the water gas-shift reaction is an exothermic reaction. The rate expression of the water gas shift reaction is written as $R_{(ii)}$. The overall redox reaction $R_{(v)}$ associates with the electric current density (j), according to Faraday's law.

Table 1. Reactions and reaction rates considered in a solid oxide fuel cell (SOFC) [38].

Reactions	No.	Reaction Equations	Reaction Rates	ΔH (kJ mol^{-1})
Steam reforming	(i)	$CH_4 + H_2O \leftrightarrow 3H_2 + CO$	$R_{(i)} = k_0 p_{CH_4} \exp\left(-\frac{E_a}{RT}\right)$	206.10
Water-gas shift	(ii)	$CO + H_2O \leftrightarrow H_2 + CO_2$	$R_{(ii)} = k_{WGSR} p_{CO}\left(1 - \frac{p_{CO_2} p_{H_2} / p_{CO} p_{H_2O}}{K_{eq}}\right)$	−41.15
Hydrogen oxidation	(iii)	$H_2 + O^{2-} \rightarrow H_2O + 2e^-$		
Oxygen reduction	(iv)	$1/2O_2 + 2e^- \rightarrow O^{2-}$		
Overall redox reaction	(v)	$H_2 + 1/2O_2 \rightarrow H_2O$	$R_{(v)} = \frac{j}{2F}$	−241.83

The lumped-parameter modeling, when only considering changes in time, is a simple approach for describing the dynamic modeling of the solid oxide fuel cell. Xi et al. [39] showed that lumped-parameter models are adequate for systems-level analysis and control through experimental validation. Moreover, the lumped model has been implemented for analysis and control of the planar SOFC systems [40]. Consequently, this work has used the lumped-parameter model for analysis, design, and control of the SOFC.

Equations (1) and (2), respectively, give the mass balances in the fuel and air channels, which provide the amount in moles of each species in the SOFC. The gas compositions in the fuel channel consist of CH_4, H_2O, CO, H_2, and CO_2, while O_2 and N_2 are the gas species in the air channel. The mass balances are:

$$\frac{dn_{i,f}}{dt} = \dot{n}_{i,f}^{in} - \dot{n}_{i,f} + \sum_{k\in\{(i),(ii),(v)\}} \upsilon_{i,k} R_k A \quad (1)$$

$$\frac{dn_{i,a}}{dt} = \dot{n}_{i,a}^{in} - \dot{n}_{i,a} + \upsilon_{i,(v)} R_{(v)} A \quad (2)$$

where $\dot{n}_{i,f}$ and $\dot{n}_{i,a}$ are the molar flow rate of species i in the fuel and air channels, respectively; $\upsilon_{i,k}$ is the stoichiometric coefficient of component i in reaction k; R_k is the rate of reaction k; and, A is a reaction area.

The temperature change within the cell is neglected for the energy balance. Equations (3) and (4) are used to compute the SOFC temperature (T_{FC}).

$$\frac{dT_{FC}}{dt} = \frac{1}{\rho_{SOFC} Cp_{SOFC} V_{SOFC}}\left(\dot{Q}_{f,in} - \dot{Q}_{f,out} + \dot{Q}_{a,in} - \dot{Q}_{a,out} + \sum_{k\in\{(i),(ii),(v)\}} (-\Delta H)_k R_k A - jAV_{FC}\right) \quad (3)$$

$$\dot{Q}_i = \sum_j \dot{n}_j Cp_j (T_i - T_{ref}) \quad (4)$$

where $\dot{Q}_i$ is the enthalpy flow in/out each fuel cell channel.

2.2. Electrochemical Model

The Nernst equation explained the difference between the thermodynamic potentials of the electrode reactions is used (Equation (5)) to determine the reversible cell voltage or theoretical open-circuit voltage (E_{OCV}).

$$E_{OCV} = E_0 - \frac{RT_{FC}}{2F} \ln\left(\frac{p_{H_2O}}{p_{H_2} p_{O_2}^{0.5}}\right) \quad (5)$$

where E_0 is the open-circuit potential at the standard pressure, which is related to the SOFC temperature, as shown in Equation (6) [41].

$$E_0 = 1.253 - 2.4516 \times 10^{-4} T_{FC}(\mathrm{K}) \tag{6}$$

When an external load is combined, the actual voltage (V_{FC}) is lower than the open-circuit voltage, owing to the voltage losses: ohmic losses (η_{Ohm}), concentration overpotentials (η_{conc}), and activation overpotentials (η_{act}), which rely on the SOFC temperature, current density, and fuel compositions. Consequently, the cell voltage can be calculated by subtracting the open-circuit voltage with the voltage drops due to the various losses from the theoretical open circuit voltage, as reported by Aguiar et al. [23]:

$$V_{FC} = E_{OCV} - (\eta_{\mathrm{Ohm}} + \eta_{\mathrm{conc}} + \eta_{\mathrm{act}}) \tag{7}$$

$$\eta_{\mathrm{Ohm}} = j\left(\frac{\tau_{\mathrm{anode}}}{\sigma_{\mathrm{anode}}} + \frac{\tau_{\mathrm{electrolyte}}}{\sigma_{\mathrm{electrolyte}}} + \frac{\tau_{\mathrm{cathode}}}{\sigma_{\mathrm{cathode}}}\right) \tag{8}$$

$$\eta_{\mathrm{conc}} = \frac{RT_{FC}}{2F}\ln\left(\frac{p_{\mathrm{H_2O,TPB}}p_{\mathrm{H_2}}}{p_{\mathrm{H_2O}}p_{\mathrm{H_2,TPB}}}\right) + \frac{RT_{FC}}{4F}\ln\left(\frac{p_{\mathrm{O_2}}}{p_{\mathrm{O_2,TPB}}}\right) \tag{9}$$

$$p_{\mathrm{H_2,TPB}} = p_{\mathrm{H_2,f}} - \frac{RT\tau_{\mathrm{anode}}}{2FD_{\mathrm{eff,anode}}}j \tag{10}$$

$$p_{\mathrm{H_2O,TPB}} = p_{\mathrm{H_2O,f}} + \frac{RT\tau_{\mathrm{anode}}}{2FD_{\mathrm{eff,anode}}}j \tag{11}$$

$$p_{\mathrm{O_2,TPB}} = P - (P - p_{\mathrm{O_2}})\exp\left(\frac{RT\tau_{\mathrm{cathode}}}{4FD_{\mathrm{eff,cathode}}P}j\right) \tag{12}$$

$$j = j_{0,\mathrm{anode}}\left[\frac{p_{\mathrm{H_2,TPB}}}{p_{\mathrm{H_2}}}\exp\left(\frac{\alpha nF}{RT_{FC}}\eta_{\mathrm{act,anode}}\right) - \frac{p_{\mathrm{H_2O,TPB}}}{p_{\mathrm{H_2O}}}\exp\left(-\frac{(1-\alpha)nF}{RT_{FC}}\eta_{\mathrm{act,anode}}\right)\right] \tag{13}$$

$$j = j_{0,\mathrm{anode}}\left[\frac{p_{\mathrm{H_2,TPB}}}{p_{\mathrm{H_2}}}\exp\left(\frac{\alpha nF}{RT_{FC}}\eta_{\mathrm{act,anode}}\right) - \frac{p_{\mathrm{H_2O,TPB}}}{p_{\mathrm{H_2O}}}\exp\left(-\frac{(1-\alpha)nF}{RT_{FC}}\eta_{\mathrm{act,anode}}\right)\right] \tag{14}$$

$$j_{0,\{\mathrm{anode,\ cathode}\}} = \frac{RT_{FC}}{nF}k_{\{\mathrm{anode,\ cathode}\}}\exp\left(-\frac{E_{\{\mathrm{anode,\ cathode}\}}}{RT_{FC}}\right) \tag{15}$$

where τ_{anode}, $\tau_{\mathrm{electrolyte}}$, and τ_{cathode} are the thickness of the anode, electrolyte, and cathode layers, respectively; σ_{anode} and $\sigma_{\mathrm{cathode}}$ are the electronic conductivity of the anode and cathode, respectively; $\sigma_{\mathrm{electrolyte}}$ is the ionic conductivity of the electrolyte; $p_{i,\mathrm{TPB}}$ is the partial pressure of component i at three-phase boundaries (TPB); $D_{\mathrm{eff,anode}}$ stands for the effective diffusivity coefficient in the anode, while considering a binary gas mixture of H_2 and H_2O with equi-molar, counter-current, one-dimensional diffusion due to a major difference in the concentration of these two key components at TPB and flow channel that are caused by the electrochemical reaction [23]; $D_{\mathrm{eff,cathode}}$ stands for the oxygen effective diffusivity coefficient in the cathode (a binary gas mixture of O_2 and N_2) (the diffusion coefficient for the electrode is assumed to be constant [42]); α is the fraction of the applied potential that promotes the transfer coefficient, which is usually taken to be 0.5 [23]; and, n is the number of electrons that are transferred in the single elementary rate-limiting reaction step represented by the Butler–Volmer equation. The activation energies of the electrode exchange current densities ($E_{\{\mathrm{anode,\ cathode}\}}$) are 137 and 140 kJ mol^{-1} for the cathode and anode, respectively [23]. The pre-exponential factors of the cathode and anode exchange current densities ($k_{\{\mathrm{anode,\ cathode}\}}$) are 2.35×10^{11} and 6.54×10^{11} Ω^{-1} m^{-1}, respectively [23].

The power density (P) is the amount of power per unit area, which can be determined by multiplying the cell voltage by the current density, as expressed:

$$P = jV_{FC} \tag{16}$$

The fuel utilization factor (U_{fuel}) is the ratio between the total fuel consumption for electricity production and the total inlet fuel, as defined:

$$U_{\text{fuel}} = \frac{\bar{j}LW}{(8Fy^0_{\text{CH}_4} + 2Fy^0_{\text{H}_2} + 2Fy^0_{\text{CO}})F^0_{\text{fuel}}} \tag{17}$$

The air ratio (λ_{air}) is the inverse of the air utilization factor, which is defined as:

$$\lambda_{\text{air}} = \frac{y^0_{\text{O}_2}F^0_{\text{air}}}{\bar{j}LW/4F} \tag{18}$$

where L is the cell length (cm^2), W is the cell width (cm^2), $\bar{j}$ is the average current density (A cm^{-2}), F is the Faraday constant (C mol^{-1}), y^0_i is the mole fraction (–), and F^0_i is the molar flow rate (mol s^{-1}).

3. Robust Model Predictive Control

A linear time-varying (LTV) system is defined for a multi-model paradigm or polytopic uncertainty to synthesize a robust controller:

$$\begin{gathered} \mathbf{x}(k+1) = \mathbf{A}(k)\mathbf{x}(k) + \mathbf{B}(k)\mathbf{u}(k) \\ \mathbf{y}(k) = \mathbf{C}\mathbf{x}(k) \\ \begin{bmatrix} \mathbf{A}(k) & \mathbf{B}(k) \end{bmatrix} \in \Omega \end{gathered} \tag{19}$$

where $\mathbf{x}(k)$ is the state of the plant, $\mathbf{u}(k)$ is the control input, and $\mathbf{y}(k)$ is the plant output. Furthermore, the set Ω to be the polytope for polytopic systems is defined as:

$$\Omega = \text{Co}\left\{\begin{bmatrix} \mathbf{A}_1 & \mathbf{B}_1 \end{bmatrix}, \begin{bmatrix} \mathbf{A}_2 & \mathbf{B}_2 \end{bmatrix}, \ldots, \begin{bmatrix} \mathbf{A}_L & \mathbf{B}_L \end{bmatrix}\right\} \tag{20}$$

where Co represents the convex hull and $\begin{bmatrix} \mathbf{A}_i & \mathbf{B}_i \end{bmatrix}$ are the vertices in the convex hull. If the system is the nominal linear time-invariant (LTI) model, it follows that $L = 1$. For other cases, $\begin{bmatrix} \mathbf{A}(k) & \mathbf{B}(k) \end{bmatrix} \in \Omega$, being defined by L vertices as:

$$\begin{gathered} \begin{bmatrix} \mathbf{A}(k) & \mathbf{B}(k) \end{bmatrix} = \sum_{i=1}^{L} \lambda_i \begin{bmatrix} \mathbf{A}_i & \mathbf{B}_i \end{bmatrix} \\ \sum_{i=1}^{L} \lambda_i = 1, \quad 0 \le \lambda_i \le 1 \end{gathered} \tag{21}$$

The nonlinear system can be represented by a polytopic uncertain linear time-varying system. Liu [43] has shown that every trajectory ($\mathbf{x}$, $\mathbf{u}$) of a nonlinear system is a trajectory of Equation (19) for some linear time-varying system in the polytope (Ω).

3.1. Robust MPC Algorithm

In this section, the explanation of the robust constrained MPC problem that is constituted of input and output constraints integrated with linear matrix inequality (LMI) constraints is presented. At each sampling time k, a robust performance objective is a min–max problem (minimization of worst-case performance cost) in terms of the quadratic objective for the LTV system, which is given by Equation (22):

$$\begin{gathered} \min_{\mathbf{u}(k+i|k), i=0,1,\ldots,m} \quad \max_{\begin{bmatrix} \mathbf{A}(k+i) & \mathbf{B}(k+i) \end{bmatrix} \in \Omega, i \ge 0} \quad J_\infty(k) \\ J_\infty(k) = \sum_{i=0}^{\infty} \left[\mathbf{x}(k+i|k)^T \mathbf{Q}_1 \mathbf{x}(k+i|k) + \mathbf{u}(k+i|k)^T \mathbf{R}\mathbf{u}(k+i|k)\right] \end{gathered} \tag{22}$$

where $\mathbf{Q}_1 > 0$ and $\mathbf{R} > 0$ are the symmetric weighting matrices.

The optimization problem at each sample time step is formulated as a convex optimization problem that is related to linear matrix inequalities constraints [29]. The Lyapunov function $V(i,k)$, which is defined as: $V(i,k) = \mathbf{x}(k+i/k)^T \mathbf{P}(i,k)\mathbf{x}(k+i/k)$, where $\forall k, \forall i \geq 0$ and $\mathbf{P}(i,k) > 0$, is utilized to ensure stability for the MPC algorithm. It is noted that, for a vector $\mathbf{x}$, $\mathbf{x}(k/k)$ represents the state measured at real time k, and $\mathbf{x}(k+i/k)$ represents the state at prediction time $k+i$ predicted at real time k.

3.2. Off-Line Robust MPC Algorithm Using Ellipsoidal Invariant Sets

The state-feedback control law can be defined as:

$$\mathbf{u}(k+i|k) = F\mathbf{x}(k+i|k), \quad i \geq 0 \tag{23}$$

The state feedback gains F in the control law are defined as $F = Y_i Q_i^{-1}$ to stabilize the closed-loop system within the ellipsoidal invariant set $\varepsilon = \left\{\mathbf{x} | \mathbf{x}^T \mathbf{Q}^{-1} \mathbf{x} \leq 1\right\}$. The matrix variables $Q_i > 0$ and Y_i are achieved from the result of the linear objective minimization problem $J_\infty(k)$, with the upper bound γ on the worst-case MPC. The symbol $*$ represents the corresponding transpose of the lower block part of the symmetric matrices. Therefore, it is determined that:

$$\min_{\gamma, Q_i, Y_i} \gamma \tag{24}$$

subject to

$$\begin{bmatrix} 1 & * \\ x_i & Q_i \end{bmatrix} \geq 0 \tag{25}$$

$$\begin{bmatrix} Q_i & * & * & * \\ A_j Q_i + B_j Y_i & Q_i & * & * \\ Q_1^{1/2} Q_i & 0 & \gamma I & * \\ R^{1/2} Y_i & 0 & 0 & \gamma I \end{bmatrix} \geq 0, \quad j = 1, 2, ..., L \tag{26}$$

Input constraints that are limited by the process equipment impose hard constraints on the manipulated variable $\mathbf{u}(k)$. Boyd et al. [44] proposed the basic idea to handle these constraints for continuous-time systems. However, the discrete-time robust MPC is presented here, as follows:

$$\begin{bmatrix} X & * \\ Y_i^T & Q_i \end{bmatrix} \geq 0, \tag{27}$$

with

$$X_{hh} \leq u_{h,\max}^2, \quad h = 1, 2, ..., n_u \tag{28}$$

For output constraints, performance terms impose constraints on the process output y(k), as:

$$\begin{bmatrix} S & * \\ \left(A_j Q_i + B_j Y_i\right)^T C^T & Q_i \end{bmatrix} \geq 0, \tag{29}$$

with

$$S_{rr} \leq y_{r,\max}^2, \quad r = 1, 2, ..., n_y \tag{30}$$

It is noted that Equation (27) is used to guarantee input constraint satisfaction, whereas Equation (29) is used to guarantee output constraint satisfaction.

4. SOFC Operation

In this work, the SOFC models that are mentioned above are implemented and simulated while using Matlab for analysis, design, and controls study of the SOFC. The lumped parameter model of SOFC is created by the relation between mass and energy balances and is used to investigate steady state and dynamic behavior. Table 2 shows the model parameters and operating conditions for the

SOFC. Regarding the steady-state analysis of the cell voltage, power density, and cell temperature related to the current density, the SOFC is designed to be operated at a current density (j) of 0.45 A cm^{-2}, at which the SOFC efficiency is optimized [45]. Under this operating condition, the cell voltage (V_{FC}) is 0.72 V, the power density (P) is 0.32 W cm^{-2}, and the cell temperature (T_{FC}) is 1058 K.

Table 2. Model parameters and operating conditions used in SOFC simulation.

Model Parameters		
Anode effective diffusivity coefficient ($D_{\text{eff,anode}}$)	3.66×10^{-5}	m^2 s^{-1}
Cathode effective diffusivity coefficient ($D_{\text{eff,cathode}}$)	1.37×10^{-5}	m^2 s^{-1}
Electronic conductivity of anode (σ_{anode})	$9.5 \times 10^7/T_{FC} \exp(-1150/T_{FC})$	Ω^{-1} m^{-2}
Electronic conductivity of cathode (σ_{cathode})	$4.2 \times 10^7/T_{FC} \exp(-1200/T_{FC})$	Ω^{-1} m^{-2}
Ionic conductivity of electrolyte ($\sigma_{\text{electrolyte}}$)	$33.4 \times 10^3 \exp(-10{,}300/T_{FC})$	Ω^{-1} m^{-2}
Anode thickness (τ_{anode})	500	µm
Cathode thickness (τ_{cathode})	50	µm
Electrolyte thickness ($\tau_{\text{electrolyte}}$)	20	µm
Fuel channel height (h_{f})	1	mm
Air channel height (h_{a})	1	mm
Cell length (L)	0.4	m
Cell width (W)	0.1	m
Operating conditions		
Pressure (P)	1	bar
Fuel inlet temperature ($T_{\text{f}}{}^0$)	1023	K
Air inlet temperature ($T_{\text{a}}{}^0$)	1023	K
Fuel utilization factor (U_{fuel})	70%	
Air ratio (λ_{air})	8.5	
Fuel feed	S/C = 2, 10% pre-reforming	
Air feed	21% O_2, 79% N_2	

5. Results and Discussion

5.1. Dynamics of SOFC

In this part, the dynamic behavior and performance of the SOFC simulated by using nonlinear mass and energy balance equations (Section 2), coupled with initial operating conditions (Section 4), are given. By varying the current density, the inlet air and fuel temperatures, and the inlet air and fuel molar flow rates, the responses of the cell temperature and cell voltage are investigated. Figure 2 shows the open-loop response of the cell temperature and voltage that result from step changes of ±10% in the current density, the inlet air and fuel temperatures, and the inlet air and fuel molar flow rates, given in terms of velocity. It can be seen that, in the initial period between 0 and 3000 s, the cell voltage and cell temperature move to 0.72 V and 1058 K, respectively, which are the nominal operating points in the dynamic model. Step changes of +10% in each input are present during the second period. For the third period, which occurs between 6000 and 9000 s, the responses are a result of step changes of −10% in each input. The last period shows a return to the initial conditions.

As seen in Figure 2a, cell voltage depends on the cell operating temperature, which relies on the gas inlet temperatures and current density. The transient response of the cell voltage and temperature is considered by a step change in current density, with the gas inlet temperatures and molar flow rates maintaining the nominal values. The result provides that the increase of cell operating temperature is caused by an instantaneous increase in hydrogen consumption within the cell when the SOFC is operated at high current densities. In addition, the cell voltage suddenly drops, which is associating with ohmic losses, although the increase in cell temperature will ultimately decrease the activation overpotentials and the internal resistance in ohmic losses. The cell voltage is dependent on the magnitude of ohmic losses [40]. The step changes of ±10% in the inlet air and fuel temperatures are also investigated with the other inputs being kept at their nominal values (Figure 2b,c). The results show that the dynamic response of fuel cell voltage and cell temperature depend on the inlet temperatures of the fuel and air. The increase in fuel and air inlet temperatures causes an increase in

the cell temperature and voltage. However, it can be seen that the air inlet temperature significantly affects the fuel cell voltage and temperature. High air feed increases the heat input to the fuel cell, which promotes the reforming reaction rate; more H_2 generated leads to high power generation. The inlet flow rates of both air and fuel can be expressed in terms of air and fuel velocity, being calculated from air ratio and fuel utilization factor, respectively. Figure 2d,e show the transient responses of fuel cell voltage and cell temperature for step changes of ±10% in the inlet flow rate of air and fuel. All other inputs, such as the current density and the inlet temperatures of air and fuel, are kept constant. Changes in the fuel cell voltage and cell temperature are observed when the molar flow rates are changed. The increase in inlet molar flow rate of fuel causes an increase in the hydrogen production rate, which is associated with an increase in the reforming reaction rate. Heat for the reformer, which is provided by heat produced in the fuel cell, results in a decrease of the cell temperature, because of the endothermic steam reforming reaction. However, the fuel cell voltage increases due to an increase in the partial pressure of hydrogen and the partial pressure of water decreases as a result of an increase in the fuel flow rate. It is noted that the overshoots in fuel cell voltage that occurred after step changes could be attributed to numerical errors, which are generated by the discontinuity in time [19].

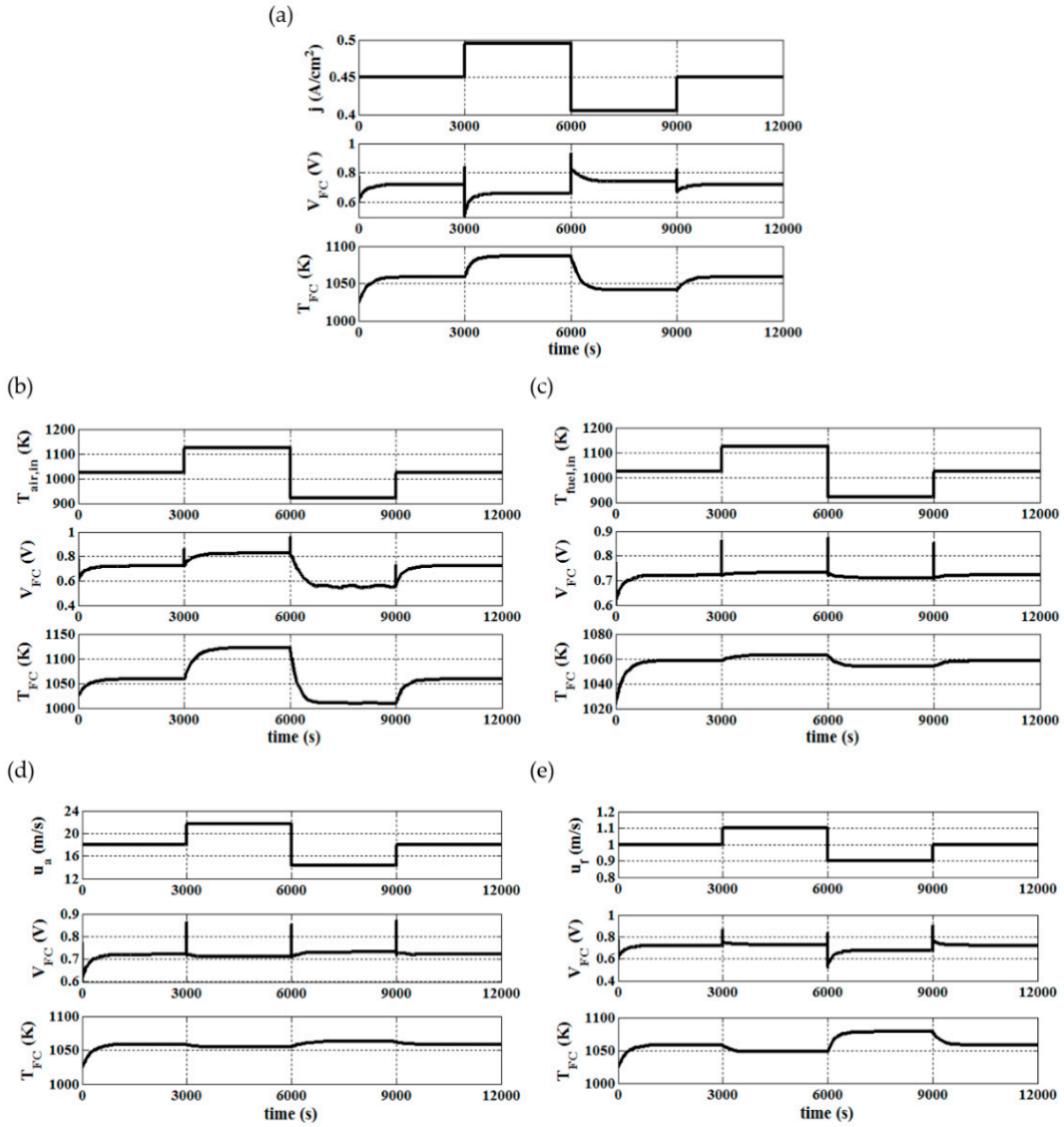

Figure 2. Voltage and cell temperature responses due to step changes in: (**a**) the current density (j); (**b**) the inlet temperature of air ($T_{\text{air,in}}$); (**c**) the inlet temperature of fuel ($T_{\text{fuel,in}}$); (**d**) the molar flow rate of air in terms of velocity (u_a); and, (**e**) the molar flow rate of fuel in terms of velocity (u_f).

5.2. Control of SOFC

In this part, the implementation of the ellipsoidal off-line robust MPC algorithm for LTV systems is presented and performed while using SeDuMi [46] and YALMIP [47]. The cell voltage (V_{FC}) is considered as the uncertainty parameter and it is assumed to be arbitrarily, varying in time within the indicated range. The lumped-parameter model of the SOFC that is represented by the nonlinear mass and energy balance ODEs is linearized, as follows:

$$\begin{aligned} \dot{\mathbf{x}} &= \mathbf{A}\mathbf{x} + \mathbf{B}\mathbf{u} \\ \mathbf{y} &= c\mathbf{x} \end{aligned} \tag{31}$$

where $\mathbf{x}$ is the state variables of the SOFC, i.e., the moles of each species in the fuel and air channels and the cell temperature, $\mathbf{u}$ is the inputs, such as the inlet molar flow rates of air and fuel, $\mathbf{A}$ and $\mathbf{B}$ are the matrices obtained from linearization, and $\mathbf{y}$ is the output variables.

Next, the linearized model is discretized while using an Euler first-order approximation in the discrete-time model expressed in Equation (32), with a sampling period of 5 s. Let $\bar{\mathbf{x}}(k) = \mathbf{x} - \mathbf{x}_{SS}$ and $\bar{\mathbf{u}}(k) = \mathbf{u} - \mathbf{u}_{SS}$, where the subscript *ss* denotes the corresponding variable at the steady-state condition, which results in the following:

$$\begin{aligned} \bar{\mathbf{x}}(k+1) &= \mathbf{A}(k)\bar{\mathbf{x}}(k) + \mathbf{B}(k)\bar{\mathbf{u}}(k) \\ \bar{\mathbf{y}}(k) &= \mathbf{c}\bar{\mathbf{x}}(k) \end{aligned} \tag{32}$$

An increase in cell temperature causes the material stresses, which is a potential problem, resulting in the anode and electrolyte material cracking. Additionally, the voltage must be controlled to make a high-efficiency SOFC. The objective is to control the cell temperature and the moles of methane at their desired values by manipulating the inlet molar flow rate of air and fuel with weighting matrices $\mathbf{Q}_1 = I$ and $\mathbf{R} = 0.1\ I$. In this study, the polytopic uncertainty model includes two vertices due to the existence of one uncertain parameter, V_{FC}. This parameter is randomly varied between 0.6 and 0.8 V in time.

Figure 3 shows the schematic diagram of the MIMO control system for the SOFC. The dashed line shows the off-line robust MPC algorithm in which the optimization problem is solved to obtain the corresponding state feedback gain, F. The solid line represents the measured on-line states at each sampling time and the corresponding state feedback control law, $\mathbf{u}$. The SOFC non-linear model is linearized (the state, input, and output variables are expressed in the deviation variables) and then discretized while using an Euler first-order approximation, which results in a discrete-time model. The uncertain parameters are implemented with the discrete-time model to generate the vertices sets. After the LTV system is obtained, it is implemented with the robust MPC algorithm. To obtain the gain F, the values of Q_i and Y_i are determined after optimization. Lastly, the state feedback control, $\mathbf{u}$, can be calculated and implemented in the control of the SOFC.

Figure 4 shows the closed-loop responses of the SOFC for the robust MPC based on the LTV systems. Figure 4a shows the closed-loop response of the cell temperature of the SOFC, whereas Figure 4b shows the closed-loop response of the moles of methane in the fuel channel. Figure 5a,b, respectively, show the control inputs of the SOFC, i.e., the inlet molar flow rates of air and fuel in velocity terms. Figure 6 shows the response of the cell voltage; the proposed MPC controller can indirectly drive the cell voltage to its desired value. The results show that when fuel cell temperature shifts from its steady-state value (1058 K), the mole fraction of methane has a slight change from the control action. The controller raises a small flow rate of fuel to reduce the temperature by enhancing the endothermic reforming reaction, which results in a slight increase in methane. In addition, the air flow is initially reduced to decrease the heat input. The robust MPC reduces the fuel flow while increasing the air flow to minimize its impact on controlled variables due to the increased methane. As a change in inputs could affect both of the controlled variables due to the inputs-outputs interaction, the MPC controller had to adjust both of the control inputs, which results in fluctuations in the initial control input profiles. The simulation results show that the proposed control algorithm obtains good

results. The MPC controller for the LTV system can maintain the cell temperature and the moles of methane at their setpoints by manipulating the inlet molar flow rates of air and fuel, respectively.

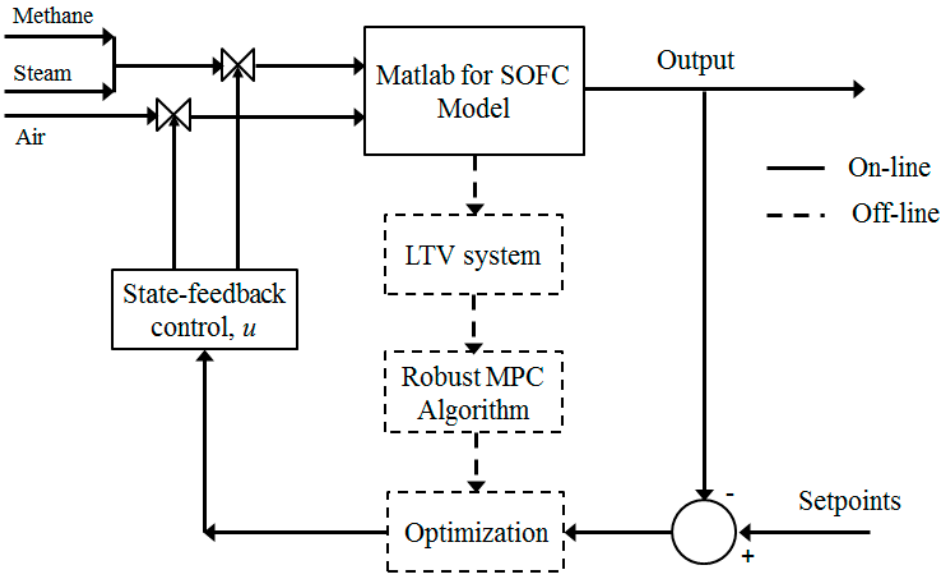

Figure 3. Schematic diagram of the control system for SOFC.

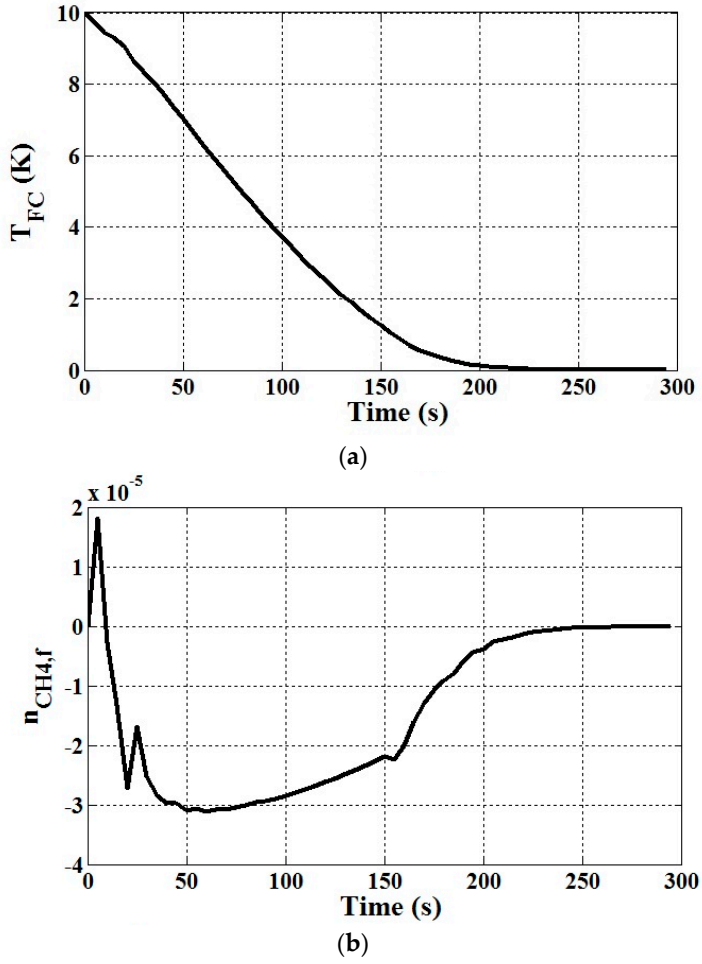

Figure 4. Closed-loop responses of SOFC: (**a**) the cell temperature of SOFC; and, (**b**) the moles of methane in fuel channel (T_{FC} and $n_{CH4,f}$ are in a deviation form).

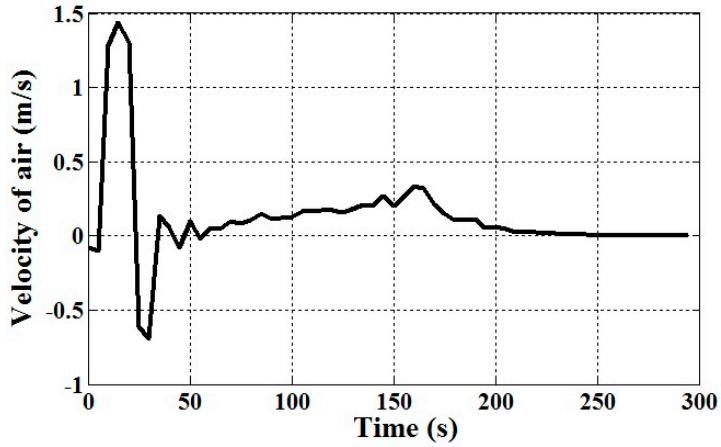

(**a**)

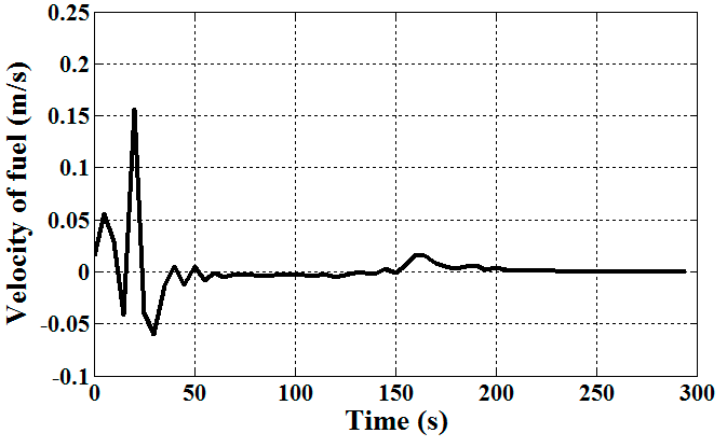

(**b**)

Figure 5. Control inputs of SOFC: (**a**) the inlet molar flow rate of air in terms of velocity; and, (**b**) the inlet molar flow rate of fuel in terms of velocity (velocities of air and fuel are in a deviation form).

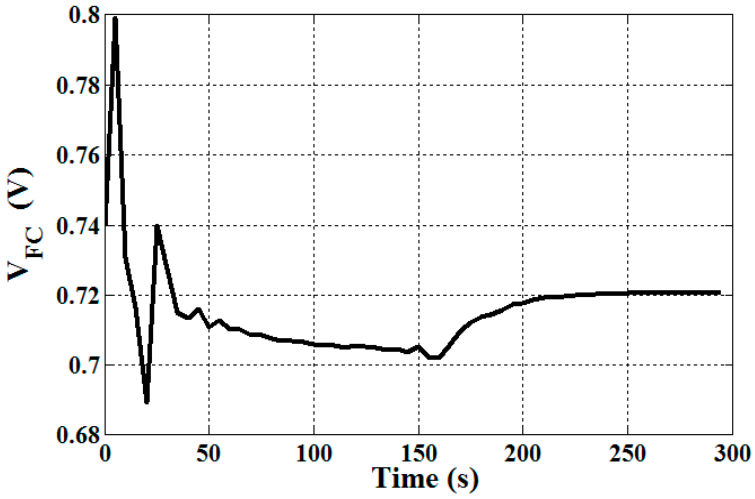

Figure 6. Closed-loop response of the cell voltage.

6. Conclusions

In this paper, an off-line robust MPC algorithm for a discrete-time LTV system with polytopic uncertainty while using the ellipsoidal invariant set was synthesized and designed for controlling a solid oxide fuel cell. The state feedback control law minimizing an upper bound on the worst-case

objective function was implemented. The lumped-parameter model was employed to explain the SOFC's dynamic behavior and design the MPC controller. In the open-loop dynamic simulations, the inlet fuel and air temperature, and the current density are related to the fuel cell temperature and voltage. Regarding the performance of the SOFC control, the off-line robust MPC algorithm can guarantee the stability of the SOFC under the model uncertainty. The controller can keep the operating temperature and the moles of methane at their setpoints by manipulating the inlet molar flow rate of air and fuel. Consequently, the cell voltage also moves to its desired value.

Author Contributions: Conceptualization, N.C. and A.A.; methodology, N.C. and A.A.; validation, N.C.; formal analysis, N.C. and A.A.; investigation, N.C.; S.K.; Y.-S.C. and A.A.; writing—original draft preparation, N.C. and A.A.; writing—review and editing, S.K.; Y.-S.C. and A.A.; supervision, S.K.; Y.-S.C. and A.A.; project administration, A.A.; funding acquisition, A.A.

Funding: This research was funded by Chulalongkorn Academic Advancement into Its 2nd Century Project, Chulalongkorn University.

Conflicts of Interest: The authors declare no conflict of interest.

References

1. Saedea, D.; Authayanun, S.; Patcharavorachot, Y.; Arpornwichanop, A. Effect of anode-cathode exhaust gas recirculation on energy recuperation in a solid oxide fuel cell-gas turbine hybrid power system. *Energy* **2016**, *94*, 218–232.
2. Atawi, I.E.; Kassem, A.M.; Zaid, S.A. Modeling, Management, and Control of an Autonomous Wind/Fuel Cell Micro-Grid System. *Processes* **2019**, *7*, 85. [CrossRef]
3. Zhao, Y.; Xia, C.; Jia, L.; Wang, Z.; Li, Y. Recent progress on solid oxide fuel cell: Lowering temperature and utilizing non-hydrogen fuels. *Int. J. Hydrog. Energy* **2013**, *38*, 16498–16517. [CrossRef]
4. Palomba, V.; Ferraro, M.; Frazzica, A.; Vasta, S.; Sergi, F.; Antonucci, V. Experimental and numerical analysis of a SOFC-CHP system with adsorption and hybrid chillers for telecommunication applications. *Appl. Energy* **2018**, *216*, 620–633. [CrossRef]
5. Fuqiang, W.; Lin, J.; Ziming, C.; Huaxu, L.; Jianyu, T. Combination of thermodynamic analysis and regression analysis for steam and dry methane reforming. *Int. J. Hydrog. Energy* **2019**, *44*, 15795–15810. [CrossRef]
6. Liao, C.H.; Horng, R.F. Experimental study of syngas production from methane dry reforming with heat recovery strategy. *Int. J. Hydrog. Energy* **2017**, *42*, 25213–25224. [CrossRef]
7. Lo Faro, M.; Trocino, S.; Zignani, S.C.; Italiano, C.; Vita, A.; Arico, A.S. Study of a solid oxide fuel cell fed with n-dodecane reformate. Part II: Effect of the reformate composition. *Int. J. Hydrog. Energy* **2017**, *42*, 1751–1757. [CrossRef]
8. Mustapha, N.A.; Sharuddin, S.S.; Zainudin, M.H.M.; Ramli, N.; Shirai, Y.; Maeda, T. Inhibition of methane production by the palm oil industrial waste phospholine gum in a mimic enteric fermentation. *J. Clean. Prod.* **2017**, *165*, 621–629. [CrossRef]
9. De Lorenzo, G.; Corigliano, O.; Lo Faro, M.; Frontera, P.; Antonucci, P.; Zignani, S.C.; Trocino, S.; Mirandola, F.A.; Aricò, A.S.; Fragiacomo, P. Thermoelectric characterization of an intermediate temperature solid oxide fuel cell system directly fed by dry biogas. *Energy Convers. Manag.* **2016**, *127*, 90–102. [CrossRef]
10. De Lorenzo, G.; Fragiacomo, P. Electrical and thermal analysis of an intermediate temperature IIR- SOFC system fed by biogas. *Energy Sci. Eng.* **2018**, *6*, 60–72. [CrossRef]
11. Triphob, N.; Wongsakulphasatch, S.; Kiatkittipong, W.; Charinpanitkul, T.; Praserthdam, P.; Assabumrungrat, S. Integrated methane decomposition and solid oxide fuel cell for efficient electrical power generation and carbon capture. *Chem. Eng. Res. Des.* **2012**, *90*, 2223–2234. [CrossRef]
12. Abdelkareem, M.A.; Tanveer, W.H.; Sayed, E.T.; Assad, M.; Allagui, A.; Cha, S.W. On the technical challenges affecting the performance of direct internal reforming biogas solid oxide fuel cells. *Renew. Sustain. Energy Rev.* **2019**, *101*, 361–375. [CrossRef]
13. Anderson, T.; Vijay, P.; Tade, M.O. An adaptable steady state Aspen Hysys model for the methane fuelled solid oxide fuel cell. *Chem. Eng. Res. Des.* **2014**, *92*, 295–307. [CrossRef]

14. Kupecki, J.; Papurello, D.; Lanzini, A.; Naumovich, Y.; Motylinski, K.; Blesznowski, M.; Santarelli, M. Numerical model of planar anode supported solid oxide fuel cell fed with fuel containing H_2S operated in direct internal reforming mode (DIR-SOFC). *Appl. Energy* **2018**, *230*, 1573–1584. [CrossRef]
15. Pret, M.G.; Ferrero, D.; Lanzini, A.; Santarelli, M. Thermal design, modeling and validation of a steam-reforming reactor for fuel cell applications. *Chem. Eng. Res. Des.* **2015**, *104*, 503–512. [CrossRef]
16. Vijay, P.; Hosseini, S.; Tade, M.O. A novel concept for improved thermal management of the planar SOFC. *Chem. Eng. Res. Des.* **2013**, *91*, 560–572. [CrossRef]
17. Vijay, P.; Tade, M.O. An adaptive non-linear observer for the estimation of temperature distribution in the planar solid oxide fuel cell. *J. Process Control* **2013**, *23*, 429–443. [CrossRef]
18. Lu, X.; Li, T.; Bertei, A.; Cho, J.I.S.; Heenan, T.M.M.; Rabuni, M.F.; Li, K.; Brett, D.J.L.; Shearing, P.R. The application of hierarchical structures in energy devices: New insights into the design of solid oxide fuel cells with enhanced mass transport. *Energy Environ. Sci.* **2018**, *11*, 2390–2403. [CrossRef]
19. Chaisantikulwat, A.; Diaz-Goano, C.; Meadows, E.S. Dynamic modeling and control of planar anode-supported solid oxide fuel cell. *Comput. Chem. Eng.* **2008**, *32*, 2365–2381. [CrossRef]
20. Madani, O.; Das, T. Feedforward based transient control in solid oxide fuel cells. *Control Eng. Pract.* **2016**, *56*, 86–91. [CrossRef]
21. Lotfi, N.; Zomorodi, H.; Landers, R.G. Active disturbance rejection control for voltage stabilization in open-cathode fuel cells through temperature regulation. *Control Eng. Pract.* **2016**, *56*, 92–100. [CrossRef]
22. Li, Y.H.; Choi, S.S. An analysis of the control and operation of a solid oxide fuel-cell power plant in an isolated system. *IEEE Trans. Energy Conver.* **2005**, *20*, 381–387. [CrossRef]
23. Aguiar, P.; Adjiman, C.S.; Brandon, N.P. Anode-supported intermediate-temperature direct internal reforming solid oxide fuel cell. II: Model-based dynamic performance and control. *J. Power Sources* **2005**, *147*, 136–147. [CrossRef]
24. Stiller, C.; Thorud, B.; Bolland, O.; Kandepu, R.; Imsland, L. Control strategy for a solid oxide fuel cell and gas turbine hybrid system. *J. Power Sources* **2006**, *158*, 303–315. [CrossRef]
25. Zhang, X.W.; Chan, S.H.; Ho, H.K.; Li, J.; Feng, Z. Nonlinear model predictive control based on the moving horizon state estimation for the solid oxide fuel cell. *Int. J. Hydrog. Energy* **2008**, *33*, 2355–2366. [CrossRef]
26. Gutierrez, G.; Ricardez-Sandoval, L.A.; Budman, H.; Prada, C. An MPC-based control structure selection approach for simultaneous process and control design. *Comput. Chem. Eng.* **2014**, *70*, 11–21. [CrossRef]
27. Wu, F. LMI-based robust model predictive control and its application to an industrial CSTR problem. *J. Process Control* **2001**, *11*, 649–659. [CrossRef]
28. Tahir, F.; Jaimoukha, I.M. Robust feedback model predictive control of constrained uncertain systems. *J. Process Control* **2013**, *23*, 189–200. [CrossRef]
29. Kothare, M.V.; Balakrishnan, V.; Morari, M. Robust constrained model predictive control using linear matrix inequalities. *Automatica* **1996**, *32*, 1361–1379. [CrossRef]
30. Bahakim, S.S.; Ricardez-Sandoval, L.A. Simultaneous design and MPC-based control for dynamic systems under uncertainty: A stochastic approach. *Comput. Chem. Eng.* **2014**, *63*, 66–81. [CrossRef]
31. Manthanwar, A.M.; Sakizlis, V.; Pistikopoulos, E.N. Robust parametric predictive control design for polytopically uncertain systems. In Proceedings of the American Control Conference, Portland, OR, USA, 8–10 June 2005; pp. 3994–3999.
32. Bumroongsri, P.; Kheawhom, S. An off-line robust MPC algorithm for uncertain polytopic discrete-time systems using polyhedral invariant sets. *J. Process Control* **2012**, *22*, 975–983. [CrossRef]
33. Pannocchia, G. Robust model predictive control with guaranteed setpoint tracking. *J. Process Control* **2004**, *14*, 927–937. [CrossRef]
34. Kouramas, K.; Varbanov, P.S.; Georgiadis, M.C.; Klemes, J.J.; Pistikopoulos, E.N. Explicit/multi-parametric model predictive control of a solid oxide fuel cell. In Proceedings of the 21st European Symposium on Computer Aided Chemical Engineering (ESCAPE21), Halkidiki, Greece, 29 May–1 June 2011; pp. 773–777.
35. Wan, Z.; Kothare, M.V. Robust output feedback model predictive control using off-line linear matrix inequalities. *J. Process Control* **2002**, *12*, 763–774. [CrossRef]
36. Pirkandi, J.; Ghassemi, M.; Hamedi, M.H.; Mohammadi, R. Electrochemical and thermodynamic modeling of a CHP system using tubular solid oxide fuel cell (SOFC-CHP). *J. Clean. Prod.* **2012**, *29–30*, 151–162. [CrossRef]
37. Yang, Y.; Du, X.; Yang, L.; Huang, Y.; Xian, H. Investigation of methane steam reforming in planar porous support of solid oxide fuel cell. *Appl. Therm. Eng.* **2009**, *29*, 1106–1113. [CrossRef]

38. Achenbach, E.; Riensche, E. Methane/steam reforming kinetics for solid oxide fuel cells. *J. Power Sources* **1994**, *52*, 283–288. [CrossRef]
39. Xi, H.; Varigonda, S.; Jing, B. Dynamic modeling of a solid oxide fuel cell system for control design. In Proceedings of the American Control Conference, Baltimore, MD, USA, 30 June–2 July 2010; pp. 423–428.
40. Murshed, A.M.; Huang, B.; Nandakumar, K. Control relevant modeling of planar solid oxide fuel cell system. *J. Power Sources* **2007**, *163*, 830–835. [CrossRef]
41. Ni, M.; Leung, M.K.H.; Leung, D.Y.C. Micro-scale modeling of oxide fuel cells with micro-structurally graded electrodes. *J. Power Sources* **2007**, *168*, 369–378. [CrossRef]
42. Patcharavorachot, Y.; Arpornwichanop, A.; Chuachuensuk, A. Electrochemical study of a planar solid oxide fuel cell: Role of support structures. *J. Power Sources* **2008**, *177*, 254–261. [CrossRef]
43. Liu, R.W. Convergent systems. *IEEE Trans. Autom. Control* **1968**, *13*, 384–391.
44. Boyd, S.; Ghaoui, L.E.; Feron, E.; Balakrishnan, V. *Linear Matrix Inequalities in System and Control Theory*; SIAM Studies in Applied Mathematics: Philadelphia, PA, USA, 1994.
45. Georgis, D.; Jogwar, S.S.; Almansoori, A.S.; Daoutidis, P. Design and control of energy integrated SOFC systems for in situ hydrogen production and power generation. *Comput. Chem. Eng.* **2011**, *35*, 1691–1704. [CrossRef]
46. Sturm, J.F. Using Sedumi 1.02, a MATLAB toolbox for optimization over symmetric cones. *Optim. Methods Softw.* **1999**, *11*, 625–653. [CrossRef]
47. Lofberg, J. YALMIP: A toolbox for modeling and optimization in MATLAB. In Proceedings of the IEEE International Symposium on Robotics and Automation, New Orleans, LA, USA, 2–4 September 2004; pp. 284–289.